INTERNATIONAL JOURNAL FOR NUMERICAL METHODS IN ENGINEERING, VOL. 37, 3441–3465 (1994)

A TEMPERATURE-BASED FORMULATION FOR FINITE ELEMENT ANALYSIS OF GENERALIZED PHASE-CHANGE PROBLEMS

DIEGO CELENTANO, EUGENIO OÑATE AND SERGIO OLLER

International Center for Numerical Methods in Engineering, E.T.S. d'Enginyers de Camins, Canals i Ports, Universitat Politècnica de Catalunya Gran Capità s/n, Mòdul C1, 08034 Barcelona, Spain

SUMMARY

A finite element formulation for solving multidimensional phase-change problems is presented. The formulation considers the temperature as the unique state variable, it is conservative in the weak form sense and it preserves the moving interface condition. In this work, an approximate jacobian matrix that preserves numerical convergence and stability is also derived. Furthermore, a comparative analysis with other different phase-change finite element techniques is performed. Finally, several numerical examples are analysed in order to show the performance of the proposed methodology.

1. INTRODUCTION

Phase-change problems appear frequently in industrial processes and other problems of technological interest. The problem is highly non-linear due to the moving interface condition and, therefore, few analytical solutions can be obtained.[1,2] Numerical solutions employing finite differences,[3,4] boundary elements,[5,6] or finite elements[7–28] techniques have been attempted by many researchers.

Among the finite element procedures two important solution techniques are found: tracking and fixed-domain methods. The first one typically uses a deforming grid formulation in order to adapt the mesh to the interface displacements.[12–13] In this context, the energy interface equation is treated in a special form. Nevertheless, this method presents many drawbacks, such as the need of starting solutions for the front position and the difficulty of dealing with appearing/disappearing phases and multiple or no-smooth interfaces, as it has been reported in.[25]

Fixed-domain methods are derived from a weak formulation that implicitly contains the moving interface condition. Within this framework, one option is to use the enthalpy as the main variable in order to take into account the latent heat effect. Once the nodal enthalpy vector is obtained for each time step, the nodal temperatures can be computed using the well-known enthalpy–temperature relationship. All enthalpy-based methods need a regularization to remove the discontinuity that appears at the phase-change front.[14–17] Rolph III and Bathe[18] and Roose and Storrer[19] use a fictitious heat source method based in the enthalpy concept. An alternative approach known as the source-based method, also derived from the enthalpy concept, has been used by Reddy and Reddy.[20] Blanchard and Fremond[21] introduce the freezing index in the energy conservation equation and solve a variational equation with the help of an homographic approximation which contains an enthalpy regularization. Other transformation methods have

CCC 0029–5981/94/203441–25$9.00

Received 15 December 1992
Revised 14 December 1993

been developed by Ichikawa and Kikuchi[22] and Lee *et al.*[23] Tamma and Railkar[24] employ the transfinite element technique in combination with the enthalpy method.

A second approach, exploited by Crivelli and his co-workers,[25–27] consists in retaining the temperature as the only state variable. In order to avoid any explicit smoothing, a special element able to integrate discontinuous functions must be used.[25–28]

The objective of this paper is to present an alternative temperature-based finite element formulation. In Section 2 the governing equations for the generalized phase-change, including the isothermal (the standard Stefan's problem) and non-isothermal cases, are presented. The weak form and the finite element formulation for the generalized phase-change problem are described in Section 3.

Convergence and stability of the numerical solution are preserved by using a new approximate jacobian matrix which is derived in Section 4. A comparative analysis with alternative techniques is performed in Section 5. Several crucial aspects of the proposed algorithm are also discussed here.

Section 6 includes several simple examples showing the effectiveness of the proposed methodology. Finally, a circular cylindrical casting test considering phase-change phenomena, temperature-dependent material properties and thermal contact effects are also analysed. Numerical results obtained for this case are compared with an existing numerical solution and some laboratory measurements.

2. GOVERNING EQUATIONS

Let an open bounded domain $\Omega \subset \mathbb{R}^{n_{\text{dim}}}$ $(1 \leqslant n_{\text{dim}} \leqslant 3)$ be the reference (initial) configuration of a non-linear heat conductor $\mathscr{B}_1$ with particles defined by $\mathbf{x} \in \bar{\Omega}$, $\Gamma = \partial\Omega$ its smooth boundary and $\Upsilon \subset \mathbb{R}^+$ be the time interval of analysis ($t \in \Upsilon$). As usual, $\bar{\Omega} = \Omega \cup \Gamma$. The 'phase-change problem' consists in finding an absolute temperature field $T: \bar{\Omega} \times \Upsilon \to \mathbb{R}^+$ such that

$$\rho_0 \frac{\partial \omega}{\partial T} \dot{T} = -\nabla \cdot \mathbf{q} + \rho_0 r \quad \text{in } \Omega \times \Upsilon \tag{1}$$

$$\omega = \hat{\omega}(\mathbf{x}, t) \quad \text{in } \Omega \times \Upsilon \tag{2}$$

$$\mathbf{q} = \hat{\mathbf{q}}(\mathbf{x}, t) \quad \text{in } \Omega \times \Upsilon \tag{3}$$

subject to the boundary conditions

$$T = \bar{T} \quad \text{in } \Gamma_T \times \Upsilon \tag{4}$$

$$\mathbf{q} \cdot \mathbf{n} = -\bar{q} - q_{\text{conv}} \quad \text{in } \Gamma_q \times \Upsilon \tag{5}$$

and the initial condition

$$T(\mathbf{x}, t)|_{t=0} = T_0(\mathbf{x}) \quad \text{in } \Omega \tag{6}$$

Equation (1) expresses the energy balance derived from the First Law of Thermodynamics (neglecting mechanical effects and volume changes[30]) where the superposed dot denotes time derivative, $\nabla(\cdot) = \partial(\cdot)/\partial\mathbf{x}$ is the gradient operator relative to a Cartesian reference system, $\rho_0: \Omega \to \mathbb{R}^+$ is the density at the reference configuration and the standard tensor notation is used in this equation.[30] Further, $\omega: \Omega \times \Upsilon \to \mathbb{R}$ is the specific internal energy, $r: \Omega \times \Upsilon \to \mathbb{R}$ the specific heat-source and $\mathbf{q}: \bar{\Omega} \times \Upsilon \to \mathbb{R}^{n_{\text{dim}}}$ the heat flux vector. The superposed caret in $\hat{\omega}$ and $\hat{\mathbf{q}}$ distinguishes these functions from their values in the constitutive equations (2) and (3), respectively.

For the isothermal phase-change case, Ω can be decomposed at any time t into two subdomains: (a) a solid phase Ω_s and (b) a liquid phase Ω_l, such that $\mathbf{x} \in \Omega_s$ if $T(\mathbf{x}, t) \leqslant \bar{T}_m$ and $\mathbf{x} \in \Omega_l$ if $T(\mathbf{x}, t) > \bar{T}_m$, where the moving interface Γ_{pc} separates both phases (Figure 1). On the other hand, for the non-isothermal phase-change case, Ω can be decomposed at any time t into three subdomains: (a) a solid phase Ω_s, (b) a mushy phase Ω_m and (c) a liquid phase Ω_l, such that $\mathbf{x} \in \Omega_s$ if $T(\mathbf{x}, t) \leqslant \bar{T}_s$, $\mathbf{x} \in \Omega_m$ if $\bar{T}_s < T(\mathbf{x}, t) \leqslant \bar{T}_l$ and $\mathbf{x} \in \Omega_l$ if $T(\mathbf{x}, t) > \bar{T}_l$ (Figure 1).

In equation (4), Γ_T is the part of the boundary where the temperature $\bar{T}$ is prescribed, while in equation (5) Γ_q, with unit outward normal $\mathbf{n}$, is the region where the normal heat flux is applied: (a) $\bar{q}$ is the prescribed normal heat flux and (b) q_{conv} is the normal heat flux due to convection–radiation phenomena. For this last term, the standard Newton's constitutive law is adopted:

$$q_{conv} = -h(T - T_{env}) \tag{7}$$

where h is the temperature-dependent convection–radiation coefficient and T_{env} is the environmental temperature (defined outside Ω). In a general case, T_{env} is the temperature at the boundary of another body $\mathscr{B}_2$, and equation (7) is the constitutive law of the medium that separates both bodies. The boundary condition (5) is of mixed type, but becomes of Neumann type when $q_{conv} = 0$. As usual, the conditions: $\bar{\Gamma}_T \cup \bar{\Gamma}_q = \partial\bar{\Omega}$ and $\Gamma_T \cap \Gamma_q = \emptyset$ are assumed to hold.

In phase-change problems, the specific internal energy is defined as[1]

$$\omega = \int_{T_{ref}}^{T} c\,\mathrm{d}T + Lf_{pc} \quad \text{in } \Omega \times \Upsilon \tag{8}$$

where T_{ref} is a reference temperature, c is the specific heat capacity, L is the latent heat released in a freezing problem (or absorbed in a melting one) and f_{pc} is the 'phase-change function' defined by

$$f_{pc}(T) = \begin{cases} 0, & T \leqslant \bar{T}_m \\ 1, & T > \bar{T}_m \end{cases} \tag{9a}$$

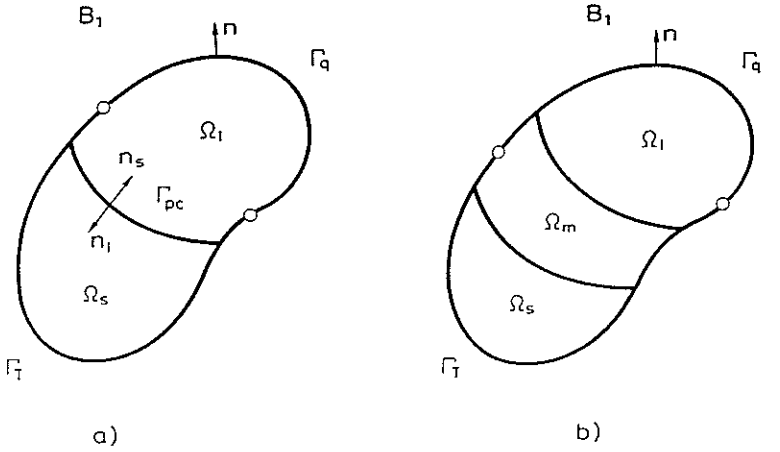

Figure 1. Geometric description of a non-linear heat conductor $\mathscr{B}_1$ for phase-change problems: (a) isothermal case; (b) non-isothermal case

for the isothermal case, and

$$f_{pc}(T) = \begin{cases} 0, & T \leqslant \bar{T}_s \\ 0 < g(T) \leqslant 1, & \bar{T}_s < T \leqslant \bar{T}_l \\ 1, & T > \bar{T}_l \end{cases} \tag{9b}$$

for the non-isothermal one (Figure 2). In equation (9a), the melting temperature is indicated by $\bar{T}_m$ while in equation (9b), $\bar{T}_s$ and $\bar{T}_l$ denote the 'solid' and 'liquid' temperatures, respectively. Further, function $g(T)$ in equation (9b) may be obtained using a microstructure model.[17] However, from a macroscopical point of view assumed in this paper, the simplest choice for $g(T)$ is the linear one with (Figure 2):

$$g(T) = (T - \bar{T}_s)/(\bar{T}_l - \bar{T}_s), \quad \bar{T}_s < T \leqslant \bar{T}_l \tag{10}$$

For the isothermal case, equation (8) shows that the specific internal energy presents a discontinuity across the moving interface Γ_{pc}. This fact makes the problem highly non-linear. For the non-isothermal case, it can be observed that the latent heat effect appears only in Ω_m. Furthermore, in Ω_s and Ω_l the classical definition of the specific heat capacity, i.e. $c = \partial\omega/\partial T$,[1] is recovered because the temperature derivative of f_{pc} is zero in those regions for both cases.

For a full description of the problem, an appropriate constitutive law for $\mathbf{q}$ (equation (3)) is necessary. The well-known Fourier's law is adopted:

$$\mathbf{q} = -\mathbf{k}\cdot\nabla T \quad \text{in } \Omega \times \Upsilon \tag{11}$$

where $\mathbf{k}$ is the conductivity second-rank tensor (which may be temperature-dependent). As a consequence of the Second Law of Thermodynamics, this tensor must be positive semidefinite.[30]

3. WEAK FORM AND FINITE ELEMENT FORMULATION

In order to obtain the weak form of this initial boundary value problem, a space $\mathcal{V}$ of admissible test functions is defined as:

$$\mathcal{V} = \{\eta \in H^1(\Omega) | \eta = 0 \text{ on } \Gamma_T\} \tag{12}$$

where $H^1(\Omega)$ is the standard notation for the Hilbert space.[30]

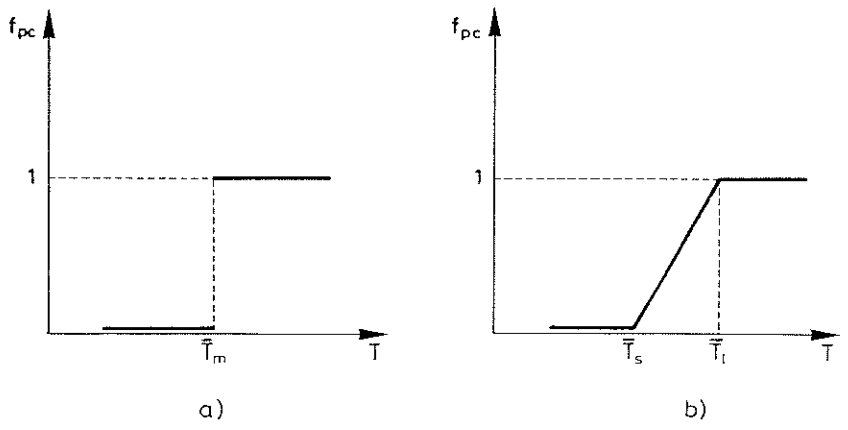

Figure 2. Phase-change function for: (a) isothermal case; (b) non-isothermal case

Furthermore, an admissible solution space ${}^t\mathscr{L}$ (for fixed time $t \in \Upsilon$) is given by

$$ {}^t\mathscr{L} = \{T(\mathbf{x}, t) \in H^1(\Omega) \mid T(\mathbf{x}, t) = \bar{T}(\mathbf{x}, t) \text{ on } \Gamma_T\} \tag{13} $$

The integral problem can be formulated as: find a temperature field $T(\mathbf{x}, t)$ that satisfies the local governing equations, such that[33]

$$ \begin{aligned} &- \langle \rho_0 c \dot{T}, \eta \rangle_\Omega - \langle \rho_0 L \dot{f}_{pc}, \eta \rangle_\Omega - \langle \mathbf{k} \cdot \nabla T, \nabla \eta \rangle_\Omega + \langle \rho_0 r, \eta \rangle_\Omega \\ &\quad + \langle \bar{q}, \eta \rangle_{\Gamma_q} - \langle h(T - T_{env}), \eta \rangle_{\Gamma_q} = 0, \quad \forall_\eta \in \mathscr{V} \end{aligned} \tag{14} $$

where $\langle \cdot, \cdot \rangle_\Omega$ and $\langle \cdot, \cdot \rangle_{\Gamma_q}$ denote the standard L_2-pairing in Ω and Γ_q, respectively ($L_2(\Omega)$ being the space of square integrable functions[29] on Ω).

Equation (14) describes the generalized phase-change problem in integral form. A further generalization takes place when two or more phase-changes ($n_{pc} \geqslant 2$) occur. For this case, the term $L\dot{f}_{pc}$ must be replaced by $\sum_{i=1}^{n_{pc}} L_i \dot{f}_{pc_i}$ (L_i and $\dot{f}_{pc_i}$ are the latent heat and the phase-change function associated with the ith phase-change, respectively) in equation (14) and subsequents equations derived in this and next sections. For simplicity in the notation, the simpler form of equation (14) is retained.

Different authors[14-19] formulate the problem as:

$$ \begin{aligned} &- \left\langle \rho_0 \left(c + L \frac{\partial f_{pc}}{\partial T} \right) \dot{T}, \eta \right\rangle_\Omega - \langle \mathbf{k} \cdot \nabla T, \nabla \eta \rangle_\Omega + \langle \rho_0 r, \eta \rangle_\Omega \\ &\quad + \langle \bar{q}, \eta \rangle_{\Gamma_q} - \langle h(T - T_{env}), \eta \rangle_{\Gamma_q} = 0, \quad \forall_\eta \in \mathscr{V} \end{aligned} \tag{15} $$

where it should be noted that in the isothermal case, the temperature derivative of f_{pc} is equal to $\delta(T - \bar{T}_m)$ (Dirac function). For numerical reasons to be discussed in Section 5, the integral equation (14) (instead of (equation 15)) will be used in this and subsequent sections. Further, an important advantage that appears when standard mathematical arguments are used for equation (14) is that the local form of the equations for the generalized phase-change problem can be recovered.[25]

To integrate in time equation (14), a generalized mid-point rule algorithm can be used.[29] Let $[t, t + \Delta t] \subset \Upsilon (\Delta t > 0)$ be a time subinterval. Assuming that algorithmic approximations of the temperature ${}^tT(\mathbf{x}): \Omega \to \mathbb{R}^+$ and temperature rate ${}^t\dot{T}(\mathbf{x}): \Omega \to \mathbb{R}$ are known, the objective is to obtain ${}^{t+\Delta t}T(\mathbf{x})$ and ${}^{t+\Delta t}\dot{T}(\mathbf{x})$. To this end, it is necessary to find ${}^{t+\Delta t}T$ which satisfies the local governing equations, such that

$$ {}^{t+\alpha\Delta t}\dot{\mathscr{X}} = ({}^{t+\Delta t}\mathscr{X} - {}^t\mathscr{X})/\Delta t \tag{16a} $$

$$ {}^{t+\alpha\Delta t}\mathscr{X} = \alpha {}^{t+\Delta t}\mathscr{X} + (1 - \alpha) {}^t\mathscr{X} \quad \text{with } \alpha \in [0, 1] \tag{16b} $$

$\mathscr{X}$ being any variable in equation (14). Choosing $\alpha = 1$ (the well-known Euler backward method), unconditional stability is achieved.[29,34]

In the context of the finite element technique,[34,35] the discrete problem can be obtained via the spatial Galerkin projection of the semidiscrete problem into a finite dimensional subspace ${}_h\mathscr{V} \subset \mathscr{V}$ of admissible C^0 continuous shape functions $N \in {}_h\mathscr{V}$. Consequently, an admissible 'algorithmic' solution space ${}^t_h\mathscr{L} \subset {}^t\mathscr{L}$ (for fixed time $t \in \Upsilon$), also consisting of typical C^0 functions, is defined.[35]

Making use of the standard spatial interpolation for the temperature field, it leads to[35]

$$ {}^t_hT(\mathbf{x}) = \mathbf{N}(\mathbf{x}) {}^t\mathbf{T}^{(e)} \tag{17} $$

with $N_i \in {}_h\mathscr{V}$ for $i = 1, \ldots, n_{node}$.

In the above, $\mathbf{N}$ is the element shape function matrix and ${}^{t}\mathbf{T}^{(e)}$ is the nodal temperature vector (the superscript e denotes element values). For simplicity in the notation, subscript h will be dropped from here onwards.

Following standard procedures, the global discretized thermal equilibrium equations can be written in matrix form as[31,32,33]

$$ {}^{t+\Delta t}\mathbf{R} = {}^{t+\Delta t}\mathbf{F} - {}^{t+\Delta t}\mathbf{C}\,{}^{t+\Delta t}\dot{\mathbf{T}} - {}^{t+\Delta t}\mathbf{K}\,{}^{t+\Delta t}\mathbf{T} - {}^{t+\Delta t}\dot{\mathbf{L}} = \mathbf{0} \tag{18} $$

where $\mathbf{F}$ is the external heat flux vector, $\mathbf{C}$ is the capacity matrix, $\mathbf{K}$ is the conductivity matrix, $\dot{\mathbf{L}}$ is the 'phase-change' vector rate and $\mathbf{R}$ is the residual vector. Once more, ${}^{t+\Delta t}\dot{\mathbf{T}}$ and ${}^{t+\Delta t}\dot{\mathbf{L}}$ are computed using equation (16a). As usual, all vectors and matrices are assembled from the element contributions in the standard manner.[34,35] The form of the different elemental expressions appearing in equation (18) can be seen in Box 1, where the superscript $\mathscr{T}$ denotes the transpose symbol, $\mathbf{F}_c$ represents the concentrated heat flux vector (temperature-dependent in a general case), and n_e is the number of loaded nodes at element e. Finally, it should be noted that the term $\dot{\mathbf{L}}$ contains the latent heat effect when $\dot{f}_{\mathrm{pc}} \neq 0$.

4. SOLUTION STRATEGY

When the residual is differentiable, an incremental iterative formulation for solving the non-linear system of equations (18) can be attempted. Therefore, the incremental iterative system can be written as[35]

$$ {}^{t+\Delta t}\mathbf{J}^{j-1}\,\Delta\mathbf{T}^{j} = {}^{t+\Delta t}\mathbf{R}^{j-1} \tag{19} $$

Box 1

Element matrices and vectors in the discretized thermal equilibrium equations

$$ \mathbf{F}^{(e)} = \int_{\Omega_q^{(e)}} \mathbf{N}^{\mathscr{T}} \rho_0 r \,\mathrm{d}\Omega + \int_{\Gamma_q^{(e)}} \mathbf{N}^{\mathscr{T}} \bar{q} \,\mathrm{d}\Gamma_q + \int_{\Gamma_q^{(e)}} \mathbf{N}^{\mathscr{T}} h T_{\mathrm{env}} \,\mathrm{d}\Gamma_q + \sum_{i=1}^{n_c} F_{ci}^{(e)} $$

$$ \mathbf{C}^{(e)} = \int_{\Omega^{(e)}} \mathbf{N}^{\mathscr{T}} \rho_0 c \,\mathbf{N} \,\mathrm{d}\Omega $$

$$ \mathbf{K}^{(e)} = \int_{\Omega^{(e)}} (\nabla \mathbf{N})^{\mathscr{T}} \mathbf{k} \,\nabla \mathbf{N} \,\mathrm{d}\Omega + \int_{\Gamma_q^{(e)}} \mathbf{N}^{\mathscr{T}} h \mathbf{N} \,\mathrm{d}\Gamma_q $$

$$ \dot{\mathbf{L}}^{(e)} = \int_{\Omega^{(e)}} \mathbf{N}^{\mathscr{T}} \rho_0 L \dot{f}_{\mathrm{pc}} \,\mathrm{d}\Omega $$

with

$$ \mathbf{L}^{(e)} = \int_{\Omega^{(e)}} \mathbf{N}^{\mathscr{T}} \rho_0 L f_{\mathrm{pc}} \,\mathrm{d}\Omega $$

$$ {}^{t+\Delta t}\mathbf{T}^{j} = {}^{t+\Delta t}\mathbf{T}^{j-1} + \Delta\mathbf{T}^{j}, \quad j = 1, \ldots, n_{\mathrm{iter}} \tag{20a} $$

$$ {}^{t+\Delta t}\mathbf{T}^{0} = {}^{t}\mathbf{T} \tag{20b} $$

where the iteration index j denotes the jth approximation to the solution in $t + \Delta t$ and the tangent

jacobian matrix is given by

$$ {}^{t+\Delta t}\mathbf{J}^{j} = -\left.\frac{{}^{t+\Delta t}\partial \mathbf{R}}{\partial \mathbf{T}}\right|^{j} \tag{21a} $$

$$ {}^{t+\Delta t}\mathbf{J}^{0} = {}^{t}\mathbf{J} \tag{21b} $$

Replacing equation (18) into equation (21a) and neglecting the contributions due to temperature-dependent thermal properties and external actions, equations (21) become

$$ {}^{t+\Delta t}\mathbf{J}^{j} \simeq {}^{t+\Delta t}\bar{\mathbf{J}}^{j} = {}^{t+\Delta t}\mathbf{K}^{j} + \left.\frac{{}^{t+\Delta t}\mathbf{C}}{\Delta t}\right|^{j} + \left.\frac{{}^{t+\Delta t}\mathbf{C}_{\mathrm{pc}}}{\Delta t}\right|^{j} \tag{22a} $$

$$ {}^{t+\Delta t}\mathbf{J}^{0} \simeq {}^{t+\Delta t}\bar{\mathbf{J}}^{0} = {}^{t}\mathbf{K} + \frac{{}^{t}\mathbf{C}}{\Delta t} + \left.\frac{{}^{t+\Delta t}\mathbf{C}_{\mathrm{pc}}}{\Delta t}\right|^{0} \tag{22b} $$

where the element contribution of the 'phase-change matrix' $\mathbf{C}_{\mathrm{pc}}$ is

$$ \mathbf{C}_{\mathrm{pc}}^{(e)} = \int_{\Omega^{(e)}} \mathbf{N}^{\mathrm{T}} \rho_0 L \frac{\partial f_{\mathrm{pc}}}{\partial T} \mathbf{N}\, \mathrm{d}\Omega \tag{23} $$

It can be observed in equation (23) that for the isothermal case the temperature derivative of f_{pc} does not exist (as mentioned above, the result is the Dirac function). Nevertheless, Storti *et al.*[27] have derived an exact tangent jacobian matrix under certain conditions over the temperature field. A different approach consists in performing an approximate numerical smoothing in order to avoid this discontinuity. One possibility is

$$ \left.{}^{t+\Delta t}\frac{\partial f_{\mathrm{pc}}}{\partial T}\right|^{j} = \frac{{}^{t+\Delta t}f_{\mathrm{pc}}^{j} - {}^{t+\Delta t}f_{\mathrm{pc}}^{j-1}}{{}^{t+\Delta t}T^{j} - {}^{t+\Delta t}T^{j-1}} \tag{24a} $$

$$ \left.{}^{t+\Delta t}\frac{\partial f_{\mathrm{pc}}}{\partial T}\right|^{0} = {}^{t}\frac{\partial f_{\mathrm{pc}}}{\partial T} \tag{24b} $$

For numerical stability conditions, a more convenient form of evaluating this derivative is

$$ \left.{}^{t+\Delta t}\frac{\partial f_{\mathrm{pc}}}{\partial T}\right|^{j} = \frac{{}^{t+\Delta t}f_{\mathrm{pc}}^{j} - {}^{t}f_{\mathrm{pc}}}{{}^{t+\Delta t}T^{j} - {}^{t}T} \tag{25a} $$

$$ \left.{}^{t+\Delta t}\frac{\partial f_{\mathrm{pc}}}{\partial T}\right|^{0} = 0 \tag{25b} $$

With these considerations, obviously $\bar{\mathbf{J}}$ is an approximate jacobian matrix and, therefore, the quadratic convergence of Newton–Raphson's method is lost. However, when solving the system of non-linear equations, the residual $\mathbf{R}$ is evaluated 'exactly' (within the numerical frame) via equation (18). Consequently, this formulation is conservative in the weak form sense.

As f_{pc} can present a jump discontinuity inside an element in the isothermal case, a non-standard spatial integration is needed to compute $\mathbf{L}$ accurately. Many researchers[25–28] have developed special integration techniques based in splitting the integral over $\Omega^{(e)}$ into $\Omega_{\mathrm{s}}^{(e)}$ and $\Omega_{\mathrm{l}}^{(e)}$ integrals, such that f_{pc} is a continuous function of T within those regions. Then, the standard Gaussian quadrature can be applied in each domain separately.

In the non-isothermal problem, the idea used in this paper is basically the same as described above but splitting the $\Omega^{(e)}$ integral into $\Omega_{n_{\mathrm{div}}}^{(e)}$ integrals (with the number of element subdivisions n_{div} fixed). Although f_{pc} is continuous in $\Omega^{(e)}$ (but with great variations, depending on the size of

the phase-change interval $(\bar{T}_l - \bar{T}_s)$), a more accurate integration is achieved using this subdomain technique.

Due to latent heat effects, a severe non-linearity is introduced in this problem. To take this fact into account, a proper convergence criterion for stopping the iteration process has to be used. The option used in this paper is written as[25,26]

$$\frac{\|^{t+\Delta t}\mathbf{R}^j\|_2}{\|^{t+\Delta t}\mathbf{K}^j\,{}^{t+\Delta t}\mathbf{T}^j\|_2} < \varepsilon_R \tag{26}$$

where $\|\cdot\|_2$ is the L_2 vector norm, and ε_R is the measure of the admissible out-of-balance residual (often taken equal to 10^{-3}).

5. COMPARISON WITH OTHER FINITE ELEMENT TECHNIQUES

Different formulations within the framework of fixed-domain methods for solving phase-change problems have been developed by many researchers in recent years. The aim of this section is to perform a brief comparative analysis between some of these techniques[14–18, 25–27] and the temperature-based formulation presented above.

5.1. Enthalpy method

Although there are different versions of this method, all of them define the enthalpy $\tilde{H}$ as a new variable such that[14–17]

$$\frac{\partial \tilde{H}}{\partial T} = c + L\frac{\partial f_{pc}}{\partial T} \tag{27}$$

where $\tilde{c} = \partial \tilde{H}/\partial T$ is usually called the equivalent specific heat capacity. Note that in fact the enthalpy variable coincides with the specific internal energy (equation (8)).

In particular, one of such versions[14–15] retains the temperature as the nodal unknown variable while the enthalpy, computed using the exact $\tilde{H}$–T curve (Figure 3), is only needed to take into account the latent heat effect via equation (27). Substituting the equivalent specific heat capacity

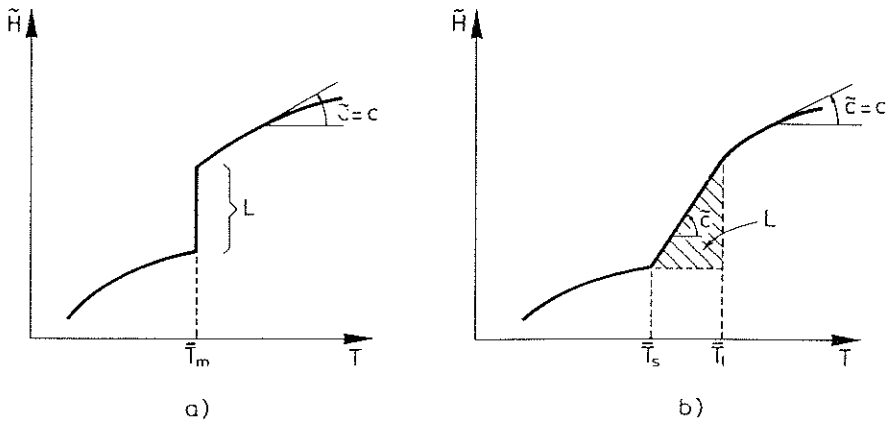

Figure 3. Exact enthalpy–temperature curve for phase-change problems: (a) isothermal case; (b) non-isothermal case

$\tilde{c}$ (equation (27)) into the generalized phase-change equation (15) and following the same procedure described in Section 3, the residual vector can be computed in this case as[14]

$$^{t+\Delta t}\tilde{\mathbf{R}} = {}^{t+\Delta t}\mathbf{F} - {}^{t+\Delta t}\tilde{\mathbf{C}}\,{}^{t+\Delta t}\dot{\mathbf{T}} - {}^{t+\Delta t}\mathbf{K}\,{}^{t+\Delta t}\mathbf{T} = \mathbf{0} \tag{28}$$

where the element contribution of $^{t+\Delta t}\tilde{\mathbf{C}}$ is

$$^{t+\Delta t}\tilde{\mathbf{C}}^{(e)} = \int_{\Omega^{(e)}} \mathbf{N}^{\mathrm{T}} \rho_0\, {}^{t+\Delta t}\tilde{c}\mathbf{N}\, \mathrm{d}\Omega \tag{29}$$

Several approximate forms have been proposed to evaluate $\tilde{c}$ when phase-change occurs.[7-11] However, due to numerical stability conditions,[14] a regularization in the H–T curve is necessary for the isothermal problem (Figure 4).

It should be noted that equation (28) involves a temperature derivative of an almost (due to the regularization) discontinuous enthalpy function, because it derives from the integral equation (15) and not from (14). Clearly, equations (27) and (28) lead to an approximate evaluation of $\tilde{c}$ and $\tilde{\mathbf{R}}$, respectively. This fact makes the method to be non-conservative in the weak form sense. Nevertheless, this drawback can be partially overcome if very small time steps are used.

As $\tilde{\mathbf{R}}$ is computed approximately, it is not useful to derive an 'exact' tangent jacobian matrix and then is usually taken in this case simply as[14]

$$^{t+\Delta t}\tilde{\mathbf{J}} = {}^{t+\Delta t}\mathbf{K} + \frac{^{t+\Delta t}\tilde{\mathbf{C}}}{\Delta t} \tag{30}$$

A modification to recover improved nodal temperatures using the exact $\tilde{H}$–T curve, after computing $\tilde{H}$ via the numerical integration of equation (27), has been proposed in.[16] For the isothermal problem, however, the moving interface condition is violated because an artificial (numerical) plateau, leading to the impossible situation of zero interface velocity, is produced. Furthermore, in this method the residual vector is calculated as described above with the inherent drawbacks mentioned.

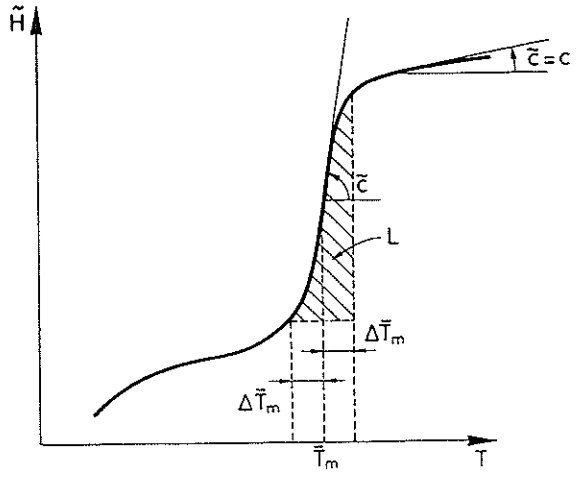

Figure 4. Regularized enthalpy–temperature curve for the isothermal phase-change problem ($2\Delta\bar{T}_m$ = regularization temperature interval)

An alternative formulation considers the nodal enthalpies as the unknowns of the problem. For this purpose, the standard spatial interpolation is now adopted for $\tilde{H}$, i.e.

$$\tilde{H}(\mathbf{x}) = \mathbf{N}(\mathbf{x})\tilde{\mathbf{H}} \tag{31}$$

with $\tilde{\mathbf{H}}$ being the nodal enthalpy vector. Furthermore, the following Taylor expansion is used:[17]

$${}^{t+\Delta t}\mathbf{T} - {}^{t}\mathbf{T} = {}^{t}\tilde{\mathbf{B}}({}^{t+\Delta t}\tilde{\mathbf{H}} - {}^{t}\tilde{\mathbf{H}}) \tag{32}$$

with

$${}^{t}\tilde{\mathbf{B}} = \frac{{}^{t}\partial \mathbf{T}}{\partial \tilde{\mathbf{H}}} \tag{33}$$

where in general $\tilde{\mathbf{B}}$ is a full matrix. In practice, however, it is assumed to be a diagonal matrix containing the enthalpy derivative of the temperature at each node. Taking into account equations (15), (27) and (32) the residual is written as[17]

$${}^{t+\Delta t}\tilde{\mathbf{R}} = {}^{t+\Delta t}\mathbf{F} - \left[\frac{{}^{t+\Delta t}\mathbf{M}}{\Delta t} + {}^{t+\Delta t}\mathbf{K}\,{}^{t}\tilde{\mathbf{B}}\right]({}^{t+\Delta t}\tilde{\mathbf{H}} - {}^{t}\tilde{\mathbf{H}}) - {}^{t+\Delta t}\mathbf{K}\,{}^{t}\mathbf{T} = \mathbf{0} \tag{34}$$

where $\mathbf{M}$ is the usual mass matrix.[35] Due to the diagonalization of $\tilde{\mathbf{B}}$, the residual vector is computed in an approximate form. After solving the non-linear system of equations, the nodal temperature vector is evaluated by means of the exact $\tilde{H}$–T curve. As it can be observed, this technique has the same drawbacks discussed above.

In this case, the simplified jacobian matrix is taken as[17]

$${}^{t+\Delta t}\tilde{\mathbf{J}} = \frac{{}^{t+\Delta t}\mathbf{M}}{\Delta t} + {}^{t+\Delta t}\mathbf{K}\,{}^{t}\tilde{\mathbf{B}} \tag{35}$$

Note that both equations (30) and (35) incorporate the latent heat effect into the jacobian matrix. This is important to avoid numerical oscillations when phase-change takes place.

To the author's knowledge, no enthalpy method evaluates the residual vector as equation (18) does. Therefore, all these methods are only nearly conservative in the weak form sense.

5.2. *Source method*

Rolph III and Bathe[18] include the non-linear effects due to phase-change in the residual as a source term $\tilde{\mathbf{Q}}$. The residual takes in this case the following form:

$${}^{t+\Delta t}\tilde{\mathbf{R}} = {}^{t+\Delta t}\mathbf{F} - {}^{t+\Delta t}\mathbf{C}\,{}^{t+\Delta t}\dot{\mathbf{T}} - {}^{t+\Delta t}\mathbf{K}\,{}^{t+\Delta t}\mathbf{T} - {}^{t+\Delta t}\tilde{\mathbf{Q}} = \mathbf{0} \tag{36}$$

When computing $\tilde{\mathbf{Q}}$, some internal constraints are imposed in order to enforce the nodal temperature vector to follow the exact $\tilde{H}$–T curve consistently with the amount of latent heat released or absorbed. Once more, the moving interface condition is violated for isothermal problems. Hence, the method is only nearly conservative in the weak form sense.

The proposed jacobian matrix in this case is[18]

$${}^{t+\Delta t}\tilde{\mathbf{J}} = {}^{t+\Delta t}\mathbf{K} \tag{37}$$

It should be noted that now the latent heat effect is not considered in $\tilde{\mathbf{J}}$.

5.3. Temperature-based methods

An important feature of these methods, which do not need any additional state variable for the numerical solution of the problem, is that the residual vector is evaluated using equation (18) (which derives from the integral equation (14)) with the consequence of being conservative in the weak form sense. Nevertheless, the most difficult task consists in finding an accurate jacobian matrix which ensures convergence and stability of the algorithm.

In the frame of quasi-Newton methods, Crivelli and Idelsohn[25] have proposed a jacobian matrix of the form:

$$^{t+\Delta t}\tilde{\mathbf{J}} = {}^{t+\Delta t}\mathbf{K} + \frac{^{t+\Delta t}\mathbf{C}}{\Delta t} + \frac{^{t+\Delta t}\mathbf{C}_{T-B}}{\Delta t} \tag{38}$$

where $\mathbf{C}_{T-B}$ is a diagonal matrix computed at nodal level which takes into account phase-change effects. It has to be noted that this equation looks like equation (22a). In fact, the temperature-based methods differ only in the evaluation procedure for $\mathbf{C}_{T-B}$.

Later, Storti *et al.*[27] have derived an exact jacobian matrix (considering constant thermal properties) for the isothermal problem. Its expression is similar to equation (38), but in this case the $\mathbf{C}_{T-B}$ contribution only exists for those elements containing the moving interface.

In the temperature-based formulation presented in this paper, the phase-change term in the jacobian matrix is only contributed by elements experiencing the phase-change effect during the time increment for which equations (25) are used for the temperature derivative of f_{pc}. This fact makes the algorithm to be stable even in the isothermal case. It should be noted that this is not the case if equations (24) are considered. In other words, the evaluation of the temperature derivative of f_{pc} via equations (25) ensures numerical stability and a reasonable convergence rate.

6. NUMERICAL EXAMPLES

6.1. Unidimensional example: convergence tests

A very simple example has been analysed first in order to test the effectiveness of the proposed solution algorithm. The problem consists of a rod of unit values of length, density, specific heat capacity and conductivity (all in consistent units) with melting temperature $\bar{T}_m = -1°C$ and initially at $T_0(x) = 0°C$. At $t = 0$ the temperature on $x = 0$ is prescribed to $\bar{T} = -2°C$ and adiabatic conditions are assumed on $x = 1$ m. In the numerical analysis, one two-noded linear finite element has been used with the normalized residual error taken as $\varepsilon_R = 10^{-6}$.

Figures 5 and 6 show comparative histograms for the number of iterations necessary for convergence of the iterative algorithm given in Section 4, where the jacobian matrix is computed using equations (22) in addition with equations (25) for evaluating the temperature derivative of f_{pc}. This problem has been analysed using different latent heat values and time steps, and therefore, each histogram represents an experiment for a given L and Δt. The columns of each histogram correspond to successive time steps for the same experiment. The standard Newton–Raphson method shown in Section 4 has been used without any special numerical technique to improve the convergence rate.

From Figures 5 and 6, it can clearly be noted that the proposed jacobian matrix gives a reasonable convergence rate in these cases. Furthermore, it is important to note that the numerical convergence cannot be achieved not even for the first time step in all cases when the contribution of $\mathbf{C}_{pc}$ is neglected. Therefore, it is possible to conclude that the consideration of the

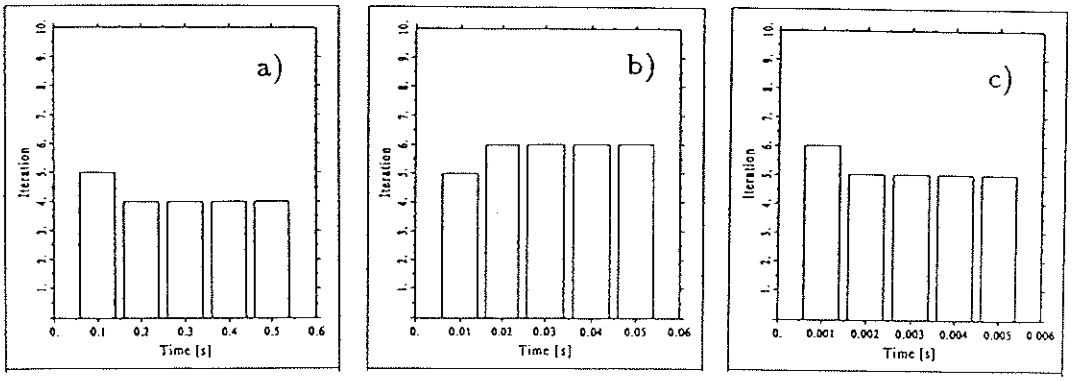

Figure 5. 1-D phase-change example: convergence rate for $L = 1{\cdot}0$ with: (a) $\Delta t = 0{\cdot}1$, (b) $\Delta t = 0{\cdot}01$ and (c) $\Delta t = 0{\cdot}001$

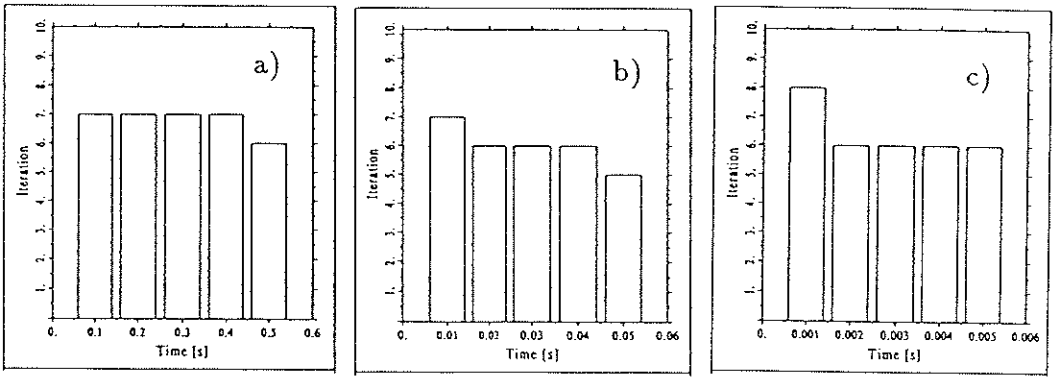

Figure 6. 1-D phase-change example: convergence rate for $L = 10{\cdot}0$ with: (a) $\Delta t = 0{\cdot}1$; (b) $\Delta t = 0{\cdot}01$ and (c) $\Delta t = 0{\cdot}001$

proposed phase-change matrix into the jacobian matrix is crucial for the numerical convergence of the iterative algorithm.

6.2. *Semi-infinite slab problem*

This well-known 1-D example has been studied in References 1, 14, 18, 25. A semi-infinite slab initially in liquid state ($T_0(x) = 0°C$) is frozen with an imposed boundary condition at $x = 0$ ($T(0, t) = -45°C$). The melting temperature is $\bar{T}_m = -0{\cdot}1°C$ and the rest of the thermal properties are found in Table I.

The numerical analysis has been performed with 32 equally spaced linear two-noded isoparametric elements of 0·125 m width. The time step used was $\Delta t = 0{\cdot}2$ s with the normalized residual error taken as $\varepsilon_R = 10^{-3}$.

The temperature evolution of a point placed at $x = 1$ m is plotted in Figure 7. Figure 8 shows the front position evolution during the cooling process. Both curves show a very good agreement between the analytical and numerical results obtained with the present temperature-based formulation. Moreover, a better approximation is attained in comparison with other numerical solutions. In order to overcome the difficulties mentioned in Section 5, the enthalpy method[14]

Table I. Thermal properties

Specific heat capacity of the solid phase: $c = c_s = 1{\cdot}0$(J/kg °C)
Specific heat capacity of the liquid phase: $c = c_l = 1{\cdot}0$(J/kg °C)
Conductivity tensor of the solid phase: $k_{ij} = \delta_{ij} k_s = 1{\cdot}08$(J/m s °C)
Conductivity tensor of the liquid phase: $k_{ij} = \delta_{ij} k_l = 1{\cdot}08$(J/m s °C)
Density of the solid phase: $\rho_0 = \rho_{0s} = 1{\cdot}0$(kg/m^3)
Density of the liquid phase: $\rho_0 = \rho_{0l} = 1{\cdot}0$(kg/m^3)
Latent heat: $L = 70{\cdot}26$[J/kg]

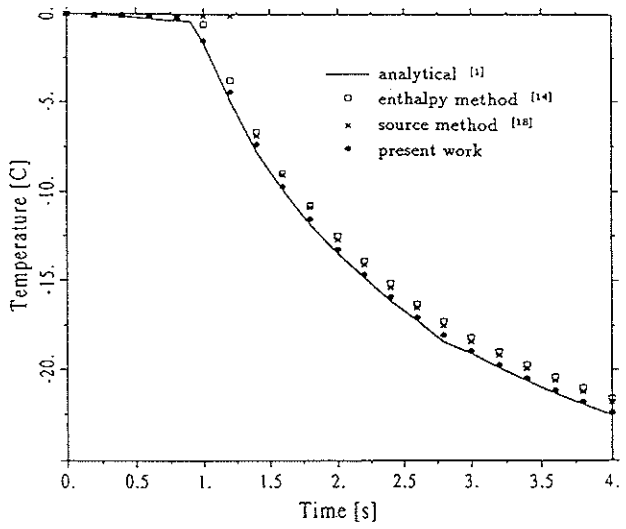

Figure 7. 1-D phase-change problem: temperature evolution at $x = 1$ m with $\bar{T}_m = -0{\cdot}1$°C

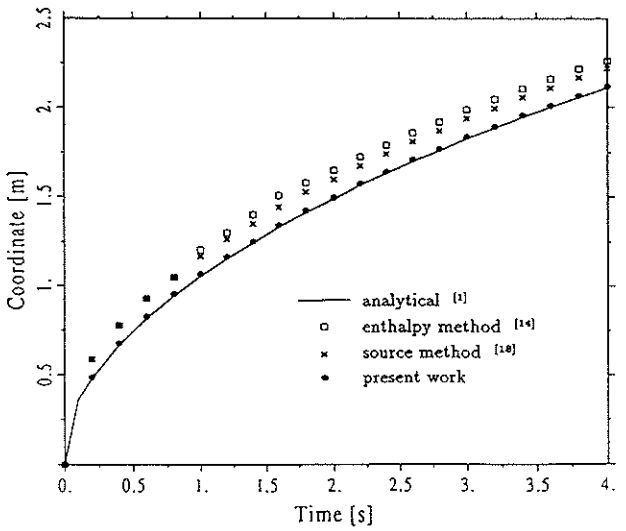

Figure 8. 1-D phase-change problem: front position evolution with $\bar{T}_m = -0{\cdot}1$°C

employs a time step of $\Delta t = 0{\cdot}01$ s with $2\,\Delta\bar{T}_m = 1°C$. In addition, an artificial plateau, corresponding to the solution given by the source method,[18] can clearly be noted in Figure 7.

The convergence rate for the first time steps is depicted in Figure 9. Similar reasonable convergence rates were observed for the rest of the analysis.

The same problem has been analysed with a melting temperature of $\bar{T}_m = -1{\cdot}0°C$. Figure 10 shows the temperature evolution at $x = 1$ m while Figure 11 depicts the front position evolution. Once more, very good agreement was found between the analytical and numerical results obtained with the present formulation. Furthermore, these curves are also compared with results

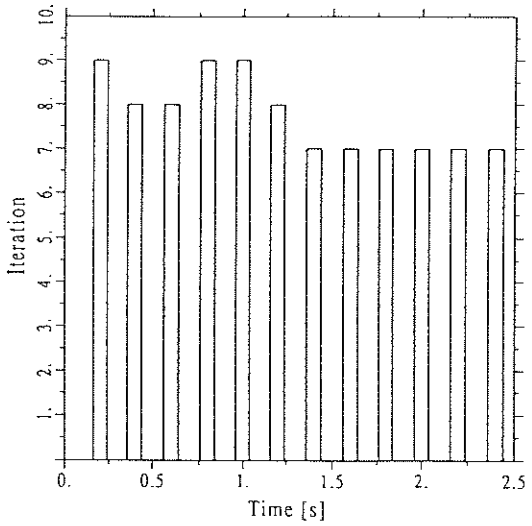

Figure 9. 1-D phase-change problem: convergence rate with $\bar{T}_m = -0{\cdot}1°C$

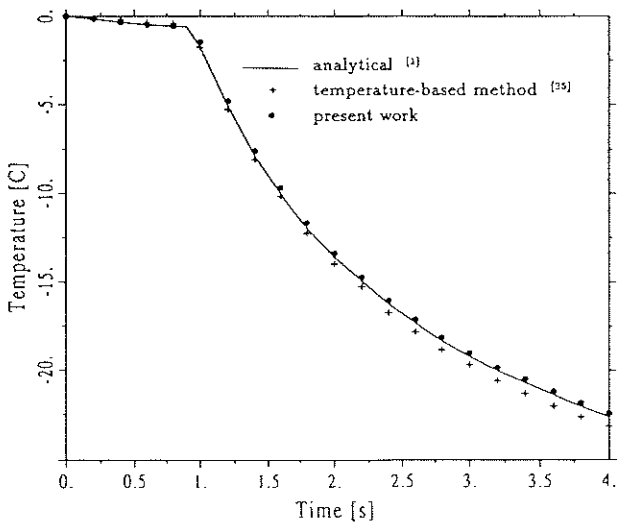

Figure 10. 1-D phase-change problem: temperature evolution at $x = 1$ m with $\bar{T}_m = -1{\cdot}0°C$

reported in Reference 25 using a temperature-based approach as well. Note that an accurate solution near the melting temperature is reached for both temperature-based formulations.

This problem has also been studied considering a phase transition temperature interval of 10°C, with $\bar{T}_s = -10{\cdot}1$°C and $\bar{T}_l = -0{\cdot}1$°C. Figure 12 shows the temperature evolution at $x = 1$ m for this case. The analytical solution is not available and, therefore, numerical results are compared with those obtained using the source method.[18]

Finally, a simple assessment concerning the computational cost has been performed. All these problems have been run on a CONVEX-120 computer. The total CPU time for the first case was

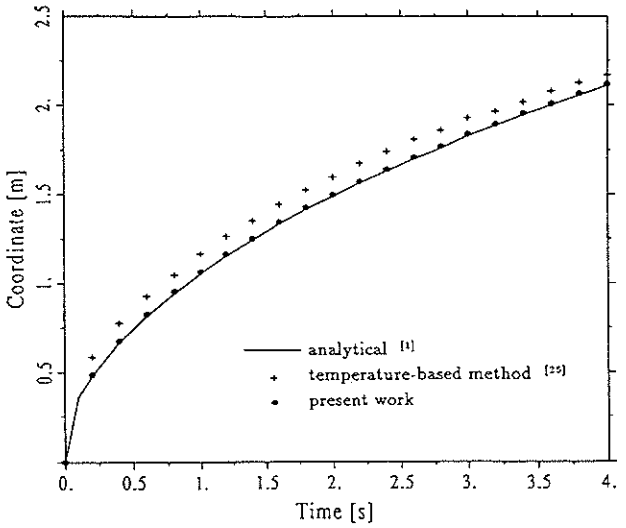

Figure 11. 1-D phase-change problem: front position evolution with $\bar{T}_m = -1{\cdot}0$°C

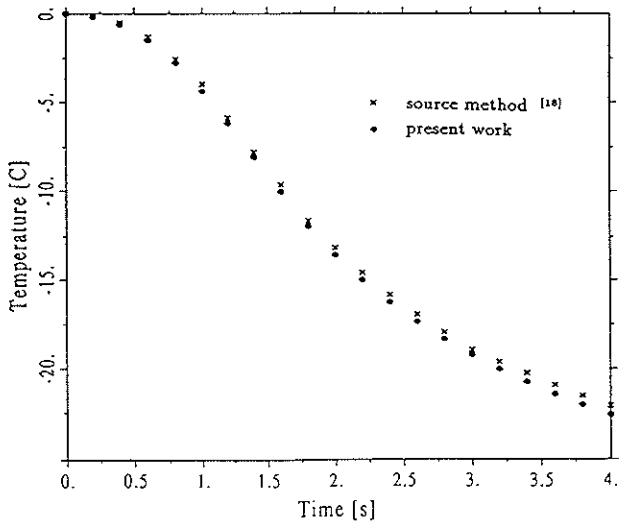

Figure 12. 1-D phase-change problem: temperature evolution at $x = 1$ m with $\bar{T}_s = -10{\cdot}1$°C and $\bar{T}_l = -0{\cdot}1$°C

56 s, where the time required to compute the phase-change matrix was 6 s. Therefore, the additional cost is about 11 per cent.

For the second case, the computational expense is similar to the former. Finally, for the non-isothermal case, the total CPU time was 35 s while the time necessary to evaluate $\mathbf{C}_{pc}$ was 1·5 s(~ 4 per cent). As expected, this last problem is, from a numerical point of view, simpler than the isothermal cases previously studied.

6.3. *Two-dimensional problem*

A two-dimensional example has also been analysed.[1,8,18,24,25,26] A semi-infinite region, initially at 0·3°C, is frozen by lowering the temperature on the side $y = 0$ to -1°C. The thermal properties are given in Table II.

Since the problem is symmetric along the line $x = y$, the analysis is restricted to the region $y \geqslant 0$ and $x \geqslant y$, imposing adiabatic conditions on the mentioned line. To simulate the infinite region, adiabatic conditions have also been imposed on the other two boundaries. With these considerations, the geometry and the finite element mesh used are plotted in Figure 13. Four-noded bilinear isoparametric elements have been used in the computations with $\Delta t = 0{\cdot}01$ s and $\varepsilon_R = 10^{-3}$.

Table II. Thermal properties

Specific heat capacity of the solid phase: $c = c_s = 1{\cdot}0$(J/kg °C)
Specific heat capacity of the liquid phase: $c = c_l = 1{\cdot}0$(J/kg °C)
Conductivity tensor of the solid phase: $k_{ij} = \delta_{ij} k_s = 1{\cdot}0$(J/m s °C)
Conductivity tensor of the liquid phase: $k_{ij} = \delta_{ij} k_l = 1{\cdot}0$(J/m s °C)
Density of the solid phase: $\rho_0 = \rho_{0s} = 1{\cdot}0$(kg/m^3)
Density of the liquid phase: $\rho_0 = \rho_{0l} = 1{\cdot}0$(kg/m^3)
Latent heat: $L = 0{\cdot}25$[J/kg]
Melting temperature: $\bar{T}_m = 0{\cdot}0$(°C).

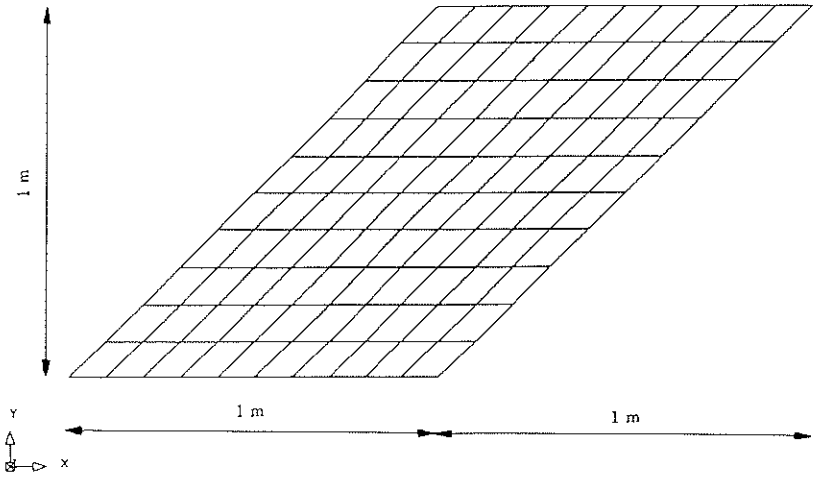

Figure 13. 2-D phase-change problem: geometry and finite element mesh

Two temperature profiles along the line $x = y$ for $t = 0{\cdot}04$ s and $t = 0{\cdot}08$ s are shown in Figures 14 and 15, respectively. Figure 16 depicts the front position evolution along the same line $x = y$. Figure 17 shows the temperature evolution at $x = y = 0{\cdot}5$ m and Figure 18 represents the interface location for $t = 0{\cdot}04$ s. Note the excellent agreement of the results obtained with the proposed formulation and the analytical solutions.[1] Numerical results using the enthalpy method,[8,24] source method[18] and an alternative temperature-based approach[25,26] are also plotted for comparison.

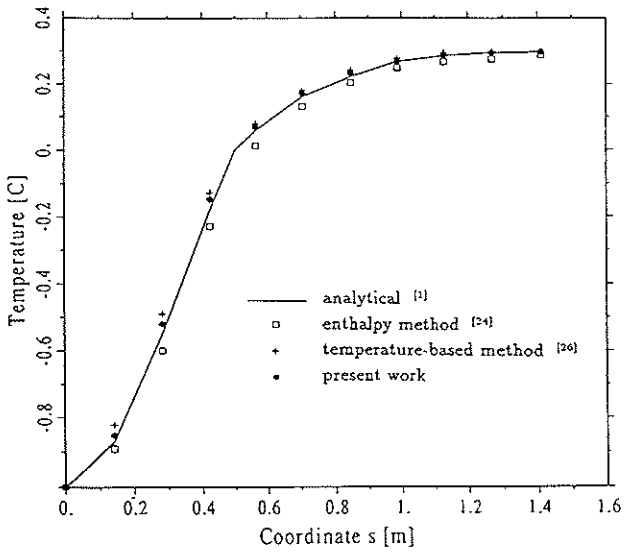

Figure 14. 2-D phase-change problem: temperature profile along $x = y$ for $t = 0{\cdot}04$ s

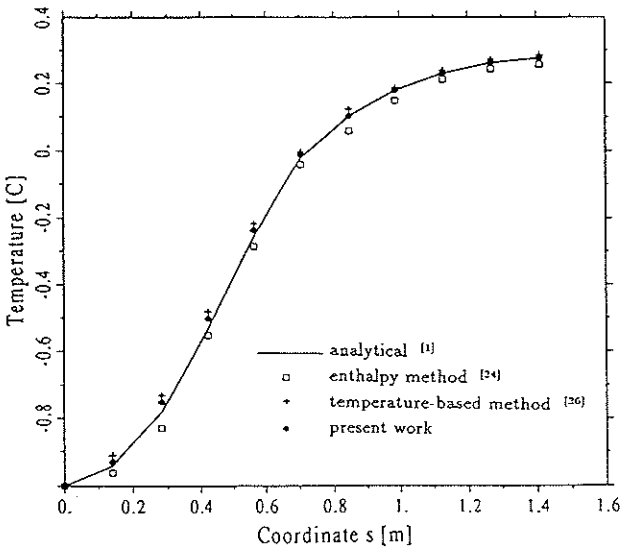

Figure 15. 2-D phase-change problem: temperature profile along $x = y$ for $t = 0{\cdot}08$ s

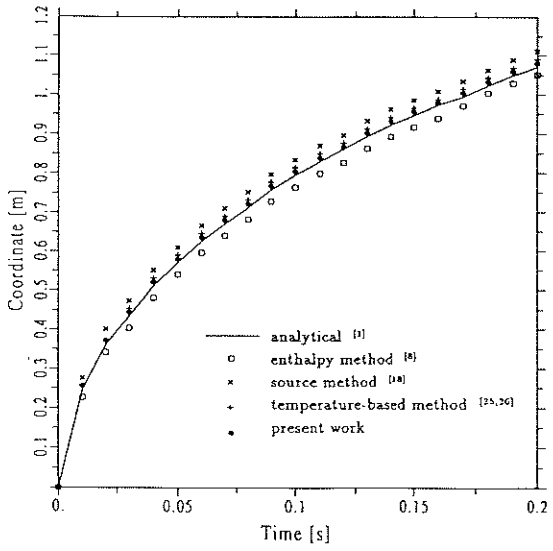

Figure 16. 2-D phase-change problem: front position evolution along $x = y$

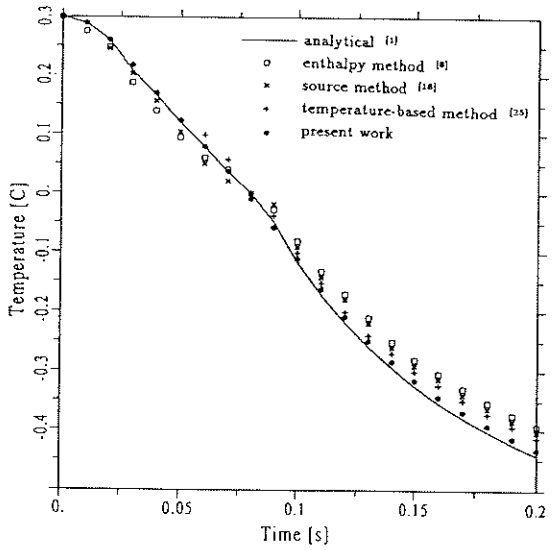

Figure 17. 2-D phase-change problem: temperature evolution at $x = y = 0{\cdot}5\,\mathrm{m}$

Figure 19 shows the convergence rate for the first time steps. The relatively low number of iterations per time step shows the effectiveness of this approach.

Finally, the total CPU time for this problem was 164 s, while the time necessary to compute $\mathbf{C}_{pc}$ was 13 s($\sim$ 8 per cent).

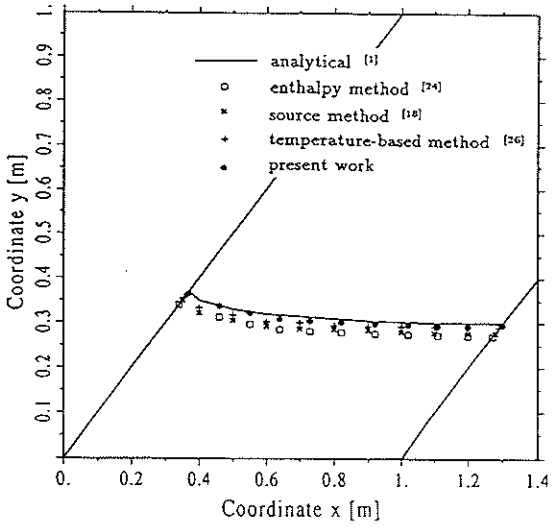

Figure 18. 2-D phase-change problem: interface location for $t = 0{\cdot}04$ s

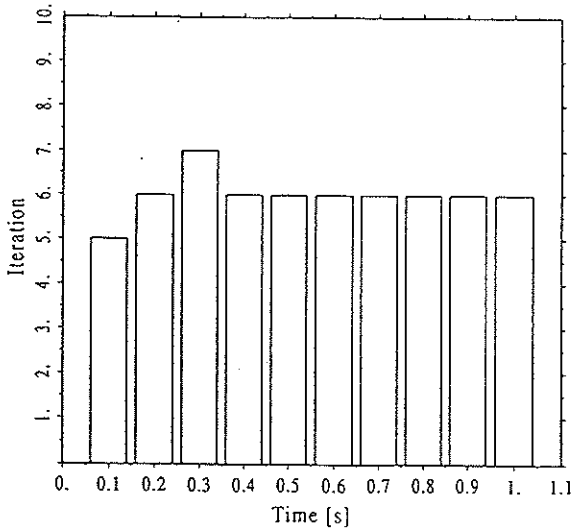

Figure 19. 2-D phase-change problem: convergence rate

6.4. Solidification test

The circular cylindrical casting of Nishida *et al.*[36] has been studied. The experiment consisted of casting commercial purity aluminium into an instrumented steel mould. Thermocouples were placed at the centre of the casting and at the casting-mould interface (Figure 20) in order to measure temperature evolutions at such points.

The temperature-dependent material properties of aluminium are shown in Table III. It should be noted that for this kind of aluminium, only an isothermal liquid–solid phase-change can occur.

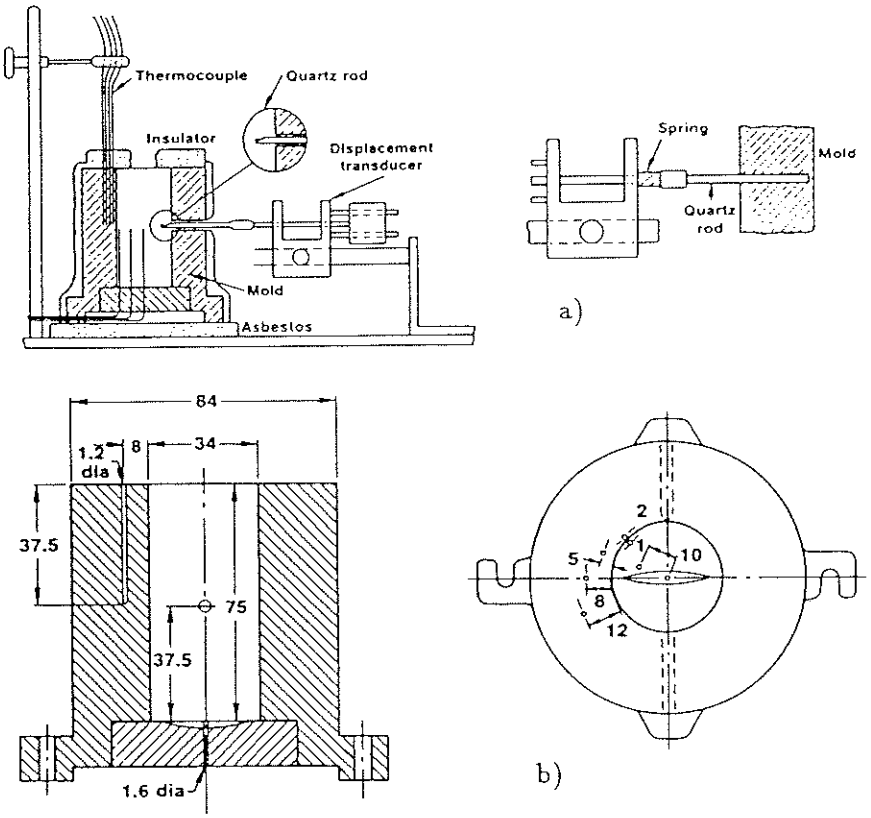

Figure 20. Solidification test: (a) schematic of the experimental set-up of Nishida *et al.*[36] and (b) geometry and thermocouple locations (drawings from Reference 37)

The steel is assumed to have constant material properties (Table IV). The convection–radiation coefficient of the casting-mould interface is shown in Table V and it is considered as temperature-dependent in order to take into account the effect of gap formation when the aluminium starts to solidify.[36]

The numerical analysis begins when the mould is completely filled with aluminium in liquid state. The initial temperatures are assumed to be 670°C for the casting and 200°C for the mould. The time step used was $\Delta t = 5$ s and the normalized residual error was taken as $\varepsilon_R = 10^{-3}$.

Three different finite element meshes have been used to study this problem. Firstly, the problem has been analysed using a 2-D finite element mesh, composed of linear triangular axisymmetric elements, shown in Figure 21(a). A second option consists in assuming that the temperature depends exclusively on the radial co-ordinate and time. In this case, a horizontal slice of unit height at the midheight of the mould has been chosen for the analysis. The corresponding finite element mesh, containing forty-two four-noded bilinear axisymmetric elements, is shown in Figure 21(b). In accordance with this simplifying assumption, a quarter of a 3-D strip has also been considered for the numerical analysis. The 3-D finite element mesh is depicted in Figure 21(c) and it has been discretized with nearly 600 linear tetrahedral elements.

Table III. Thermal properties of aluminium

Density

$$\rho_0 = 2650{\cdot}0(\text{kg/m}^3)$$

Specific heat capacity

$c(T)$(kcal/kg °C)	T(°C)
0·2283	100·0
0·2379	200·0
0·2476	300·0
0·2576	400·0
0·2672	500·0
0·2769	600·0

Conductivity coefficient

$k(T)$(kcal/m s °C)	T(°C)
0·0560	100·0
0·0540	200·0
0·0530	400·0
0·0520	600·0
0·0500	659·9
0·0220	660·1
0·0230	800·0

Melting temperature

$$\bar{T}_m = 660{\cdot}0(°\text{C})$$

Latent heat

$$L = 94{\cdot}44(\text{kcal/kg})$$

The variations of $c(T)$ and $k(T)$ have been assumed to be piecewise linear within the mentioned temperature.

Table IV. Thermal properties of steel

Density: $\rho_0 = 7850{\cdot}0(\text{kg/m}^3)$

Specific heat capacity:

$$c = 0{\cdot}1320(\text{kcal/kg °C})$$

Conductivity coefficient:

$$k = 0{\cdot}0109(\text{kcal/m s °C})$$

Table V. Thermal properties of the casting-mould interface

Convection-radiation coefficient:

$hx10^7$(kcal/m² s °C)	T(°C)
7·00	$\geqslant$ 660·0
1·00	$<$ 660·0

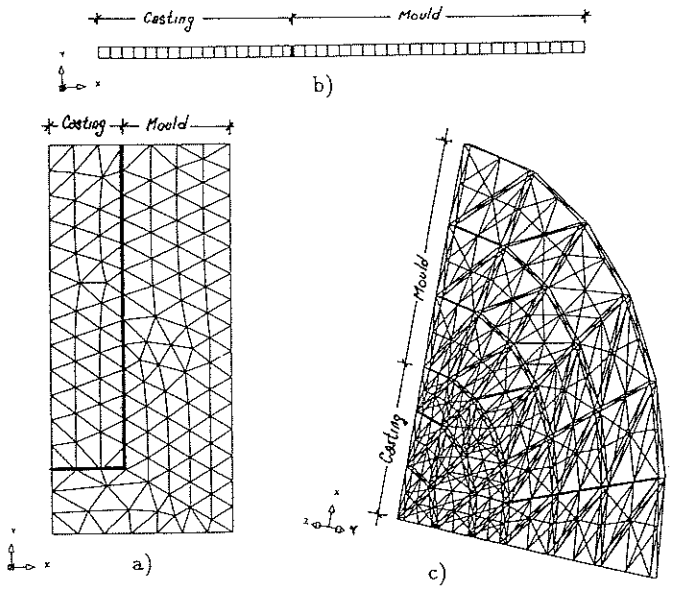

Figure 21. Solidification test: finite element meshes: (a) complete model with triangular axisymmetric elements, (b) 2-D strip with bilinear axisymmetric elements and (c) a quarter of a 3-D strip with tetrahedra elements

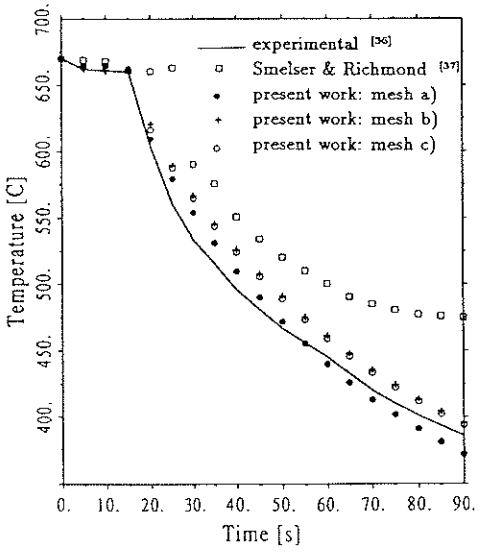

Figure 22. Solidification test: temperature evolution at the centre

The temperature evolution at the centre of the casting, at the outer casting surface and at the inner mould surface are plotted in Figures 22, 23 and 24, respectively. A good agreement between numerical results obtained with the present formulation and experimental measurements is achieved. The phase-change effects in the casting can clearly be noted in Figure 22. The numerical

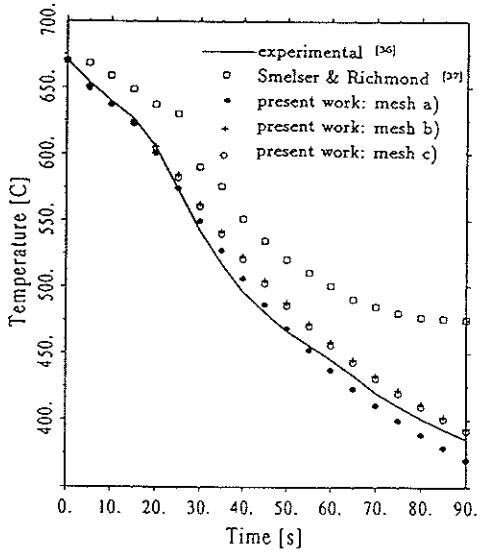

Figure 23. Solidification test: temperature evolution at the casting surface

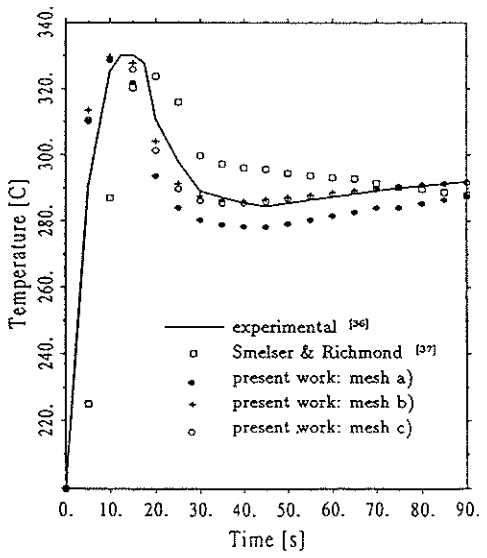

Figure 24. Solidification test: temperature evolution at the mould surface

solution given by Smelser and Richmond corresponds to the well-known apparent specific heat capacity method,[37] that poorly predicts the temperature field near the phase-change region. Finally, the simplifying assumption mentioned above seems to be relatively good, as it was already mentioned in Reference 37.

CONCLUSIONS

A temperature-based finite element formulation has been presented. The main features of such a formulation are:

(a) It is conservative in the weak form sense.
(b) It preserves the moving interface condition.
(c) It can solve generalized phase-change problems.
(d) It does not need any explicit regularization because an accurate integration technique is employed. Thus, coarser meshes and larger time steps (in comparison with other methods) can be used.
(e) It considers a proper convergence criterion.
(f) An approximate jacobian matrix has been derived. This matrix preserves numerical stability and gives a reasonable convergence rate.
(g) The numerical examples analysed show the accuracy of the present formulation and its computational efficiency.

Although a rigorous convergence and stability analyses are still lacking, numerical experiments have demonstrated that the present formulation is robust and it can accurately simulate generalized phase-change problems.

ACKNOWLEDGEMENTS

This work has been supported by RENAULT, under contract No. CIMNE/10/H5.12.603. The support provided by BRITE/EURAM Project No. BE-4596 under contract No. BREU-0443 is also gratefully acknowledged.

REFERENCES

1. H. Budhia and F. Kreith, 'Heat transfer with melting or freezing in a wedge', *Int. J. Heat Mass Transfer*, **16**, 195–211 (1973).
2. L. Tao, 'The Stefan problem with an imperfect thermal contact at the interface', *J. Appl. Mech. ASME*, **49**, 715–720 (1982).
3. N. Shamsundar and E. Sparrow, 'Analysis of multidimensional conduction phase change via the enthalpy model', *J. Heat Transfer ASME*, 333–340 August (1975).
4. G. Bell and A. Wood, 'On the performance of the enthalpy method in the region of a singularity', *Int. j. numer. methods eng.*, **19**, 1583–1592 (1983).
5. K. O'Neill, 'Boundary integral equation solution of moving boundary phase change problems', *Int. j. numer. methods eng.*, **19**, 1825–1850 (1983).
6. N. Zabaras and S. Mukherjee, 'An analysis of solidification problems by the boundary element method', *Int. j. numer. methods eng.*, **24**, 1879–1900 (1987).
7. M. Salcudean and Z. Abdullah, 'On the numerical modelling of heat transfer during solidification', *Int. j. numer. methods eng.*, **25**, 445–473 (1988).
8. K. Tamma and R. Namburu, 'Recent advances, trends and new perspectives via enthalpy-based finite element formulations for applications to solidification problems', *Int. j. numer. methods eng.*, **30**, 803–820 (1990).
9. V. Voller, C. Swaminathan and B. Thomas, 'Fixed grid techniques for phase change problems: a review', *Int. j. numer. methods eng.*, **30**, 875–898 (1990).
10. A. Dalhuijsen and A. Segal, 'Comparison of finite element techniques for solidification problems', *Int. j. numer. methods Eng.*, **23**, 1807–1829 (1986).
11. R. Viskanta, 'Heat transfer during melting and solidification of metals', *J. Heat Transfer ASME*, **110**, 1205–1219 (1988).
12. D. Lynch and K. O'Neill, 'Continuously deforming finite elements for the solution of parabolic problems, with and without phase change', *Int. j. numer. methods eng.*, **17**, 81–96 (1981).
13. Y. Ruan and N. Zabaras, 'An inverse finite-element technique to determine the change of phase interface location in two-dimensional melting problems', *Commun. appl. numer. methods*, **7**, 325–338 (1991).

14. K. Morgan, R. Lewis and O. Zienkiewicz, 'An improved algorithm for heat convection problems with phase change', *Int. j. numer. methods eng.*, **12**, 1191–1195 (1978).
15. G. Comini, S. Del Guidice, R. Lewis and O. Zienkiewicz, 'Finite element solution of non-linear heat conduction problems with special reference to phase change', *Int. j. numer. methods eng.*, **8**, 613–624 (1974).
16. G. Comini, S. Del Guidice and O. Saro, 'A conservative algorithm for multidimensional conduction phase change', *Int. j. numer. methods eng.*, **30**, 697–709 (1990).
17. P. Thévoz, J. Desbiolles and M. Rappaz, 'Modelling of equiaxed microstructure formation in casting', *Metall. Trans. A*, **20A**, 311–322 (1989).
18. W. Rolph III and K. Bathe, 'An efficient algorithm for analysis of nonlinear heat transfer with phase changes', *Int. j. numer. methods eng.*, **18**, 119–134 (1982).
19. J. Roose and O. Storrer, 'Modelization of phase changes by fictitious heat flow', *Int. j. numer. methods eng.*, **20**, 217–225 (1984).
20. M. Reddy and J. Reddy, 'Numerical simulation of forming processes using a coupled fluid flow and heat transfer model', *Int. j. numer. methods eng.*, **35**, 807–833 (1992).
21. D. Blanchard and M. Fremond, 'The Stefan problem: computing without the free boundary', *Int. j. numer. methods eng.*, **20**, 757–771 (1984).
22. Y. Ichikawa and N. Kikuchi, 'A one-phase multi-dimensional Stefan problem by the method of variational inequalities', *Int. j. numer. methods eng.*, **14**, 1197–1220 (1979).
23. T. Lee, S. Advani, J. Lee and H. Moon, 'A fixed grid finite element method for nonlinear diffusion problems with moving boundaries', *Comput. Mech.*, **8**, 111–123 (1991).
24. K. Tamma and S. Railkar, 'Hybrid transfinite element modelling analysis of non-linear heat conduction problems involving phase change', *Eng. Comput.*, **5**, 117–122 (1988).
25. L. Crivelli and S. Idelsohn, 'A temperature-based finite element solution for phase-change problems', *Int. j. numer. methods eng.*, **23**, 99–119 (1986),.
26. M. Storti, L. Crivelli and S. Idelsohn, 'Making curved interfaces straight in phase-changes problems.', *Int. j. numer. methods eng.*, **24**, 375–392 (1987).
27. M. Storti, L. Crivelli and S. Idelsohn, 'An efficient tangent scheme for solving phase-change problems', *Comput. Methods Appl. Mech. Eng.*, **66**, 65–86 (1988).
28. G. Steven, 'Internally discontinuous finite elements for moving interface problems', *Int. j. numer. methods eng.*, **18**, 569–582 (1982).
29. J. Simo, 'Nonlinear stability of the time-discrete variational problem of evolution in nonlinear heat conduction, plasticity and viscoplasticity', *Comput. Methods Appl. Mech. Eng.*, **88**, 111–131 (1991).
30. L. Malvern, *Introduction to the Mechanics of a Continuous Medium*, Prentice-Hall, Englewood Cliffs, N.J., 1969.
31. D. Celentano, S. Oller and E. Oñate, 'A Constitutive Thermomechanical Model for Solidification of Metals', *Journées Numériques de Besançon: Les problemes de changement de phase*, 19–30 (1991).
32. D. Celentano, S. Oller and E. Oñate, 'A plastic constitutive model to simulate the solidification in casting problems', in R. Owen, E. Oñate and E. Hinton (eds.), *Proc. Complas III*. Pineridge Press/CIMNE, Swansea, 1992, pp. 1089–1102.
33. D. Celentano, 'A thermomechanical model for solidification problems in metals', *Ph.D. Thesis*, Universitat Politècnica de Catalunya, Barcelona, Spain, 1994.
34. T. Hughes, *The Finite Element Method*, Prentice-Hall, Englewood Cliffs, N.J., 1987.
35. O. Zienkiewicz and R. Taylor, *The Finite Element Method*, 4th edn, Vol. 1 and 2, McGraw-Hill, London, 1989.
36. Y. Nishida, W. Droste and S. Engler, 'The air-gap formation process at the casting mold interface and the heat transfer mechanism through the gap', *Metall. Trans. B*, **17B**, 833–844 (1986).
37. R. Smelser and O. Richmond, 'Constitutive Model Effects on Stresses and Deformations in a Solidifying Circular Cylinder', *Modelling of Casting and Welding Processes* IV, A. F. Giamei and G. J. Abbaschian (eds.), The Minerals, Metals and Materials Society, 1988.